Available online at www.sciencedirect.com
ScienceDirect
Sensors and Actuators B 124 (2007) 192–201
SENSORS AND ACTUATORS B CHEMICAL
www.elsevier.com/locate/snb

# High temperature zirconia oxygen sensor with sealed metal/metal oxide internal reference

John V. Spirig [a,d], Ramasamy Ramamoorthy [a,d,1], Sheikh A. Akbar [b,d], Jules L. Routbort [c], Dileep Singh [c], Prabir K. Dutta [a,d,*]

[a] *Department of Chemistry, The Ohio State University, 100 West 18th Avenue, Columbus, OH 43210, United States*
[b] *Department of Materials Science and Engineering, The Ohio State University, 2041 College Road, Columbus, OH 43210, United States*
[c] *Argonne National Laboratory, 9700 South Cass Avenue, Argonne, IL 60439, United States*
[d] *The Center for Industrial Sensors and Measurement, 177 Watts Hall, 2041 College Road, Columbus, OH 43210, United States*

Received 19 June 2006; received in revised form 12 December 2006; accepted 13 December 2006
Available online 19 December 2006

**Abstract**

Potentiometric internal reference oxygen sensors are created by embedding a metal/metal oxide mixture within a yttria-stabilized zirconia oxygen-conducting ceramic superstructure. Three metal/metal oxide systems based on Pd, Ni, and Ru are examined. A static internal reference oxygen pressure is produced inside the reference chamber of the sensor at the target application temperature. The metal/metal oxide-containing reference chamber is sealed within the stabilized zirconia ceramic superstructure by a high pressure (3–6 MPa) and high temperature (1200–1300 °C) bonding method that initiates grain boundary sliding between the ceramic components. The bonding method creates ceramic joints that are pore-free and indistinguishable from the bulk ceramic. The Pd/PdO-based oxygen sensor presented in this study is capable of long-term operation and resistant to the strains of thermal cycling. The current temperature limit of the device is limited at 800 °C. As the sensor does not require reference gas plumbing there is flexibility in placement of sensors in a combustion stream. Furthermore, the sensor assembly process readily lends itself to miniaturization.
© 2007 Elsevier B.V. All rights reserved.

*Keywords:* Combustion sensor; Harsh environment; Ceramic bonding; Grain boundary sliding; Cross-sensitivity

## 1. Introduction

It is estimated that yearly savings of $409 million could be enabled through combustion optimization within coal-fired power plants [1]. In order to operate under optimal conditions, sensors that measure combustion products are required. Sensor-enabled feedback control will allow boilers to operate at peak efficiency, maximizing energy output and minimizing pollutant emissions. For optimal combustion, the levels of oxygen need to be carefully controlled. In the majority of commercial harsh environment oxygen sensors, air is provided from outside the combustion environment to a reference electrode that is separated from the sensing environment by a zirconia tube [2]. In these potentiometric tube-type sensors, the oxygen concentration differential between the pumped in gas and the measuring environment generates an open circuit potential that obeys the Nernst law, allowing for direct calculation of the unknown concentration of oxygen. Isolating and sealing an internal oxygen reference under high temperature conditions would make it possible to eliminate the need for an air reference required by state-of-the-art commercial oxygen sensors.

In the past three decades, there have been numerous attempts to replace bulky and expensive high temperature gas plumbing with innovative reference packaging. Critical to these designs is the need to prevent oxygen leaking from the reference chamber at the high temperatures encountered in combustion streams [3]. In 1975, Fouletier et al. [4] demonstrated that a metal/metal oxide mixture encapsulated within a ceramic superstructure and placed in intimate contact with a Pt electrode would generate a

* Corresponding author at: Department of Chemistry, The Ohio State University, 100 West 18th Avenue, Columbus, OH 43210, United States.
Tel.: +1 614 2924532; fax: +1 614 2920462.
*E-mail address:* dutta.1@osu.edu (P.K. Dutta).
[1] Present address: GE Advanced Materials, 5605 Granger Road, Independence, OH 44131, United States.

0925-4005/$ – see front matter © 2007 Elsevier B.V. All rights reserved.
doi:10.1016/j.snb.2006.12.022

stable oxygen pressure based on the thermodynamic equilibrium at a given temperature. In 1977, seeking to improve on the sealing which limited the applications of an internal reference device, Haaland [5] proposed that it would be possible to hot press a gastight Pt/zirconia chamber into which a known concentration of oxygen could be pumped. While simple in design, these sensors were never successfully commercialized because ceramic seals that contain intermediary bonding agents strain against mismatched thermal expansions in the course of long-term high temperature operation.

Maskell [6] points to three sources of leak that inhibit high temperature oxygen sensor operation; physical leak due to lack of hermaticity, leak due to electronic conduction through the electrolyte, and leakage due to circulating currents in the metal used for sealing. Modern variations of the internal reference oxygen sensors present in the literature tend to be based on the Fouletier et al. [4] model, but still generally fail to accommodate all three sources of leak. Recent examples of internal reference $O_2$ sensors have been put forth by Kaneko et al. [7], Zhuikov [8], and van Setten et al. [9]. Kaneko et al. [7] embeds a metal/metal oxide mixture inside a ceramic superstructure in intimate contact with the reference electrode and seals the circumference of the package with glass. Zhuikov [8] hot-presses a zirconia single crystal into a refractory ceramic tube and caps the apparatus in stainless steel, embedding a molten reference inside the sensor package. The Kaneko et al. [7] model eliminates the leak due to bonding agent/electrolyte interactions by using a metal-free glass seal, but, as the authors indicate, the sensor is still subject to failures in hermaticity due to cracks along the glass-joined circumference and electronic conduction. The authors attempt to redress this leakage through use of a pump-gauge design modification and intuitive reference choice, similar to Fouletier et al. [4]. Zhuikov [8] does not indicate how the stainless steel cap/sensor housing bond prevents the physical $O_2$ leak, but the metal in the cap is in intimate contact with the electrolyte and therefore subject to leakage through the bonding agent. van Setten et al. [9] encapsulates a metal/metal oxide mixture below pulsed laser deposition (PLD)-deposited layers of Ag, glass, then Au. This method isolates the metal/metal oxide well, but the glass used between the Au capping/electrode layer and the Ag protective layer softens at 447 °C, limiting maximum sensor temperature to below that threshold.

There are many functional internal reference designs to be found in the literature and all struggle to overcome the challenge of creating a high temperature seal that prevents the reference gas from equilibrating with the external environment. As there has yet to be an ideal solution, the challenge remains to create a hermetic seal with bonding agents that exhibit minimal thermal expansion coefficient mismatch or interfere with sensor signals. In the present study, gas leakage was eliminated by fusing a stabilized zirconia sensor package of five distinct pieces into a discrete body through a unique deformation bonding technique. The joining process using grain boundary sliding enables the creation of complex, jointless structures [10]. Grain boundary sliding is generally achieved at approximately one-half the melting temperature of the material under a load and evidenced when a small stress results in a large strain [11]. A glass seal is used to seal the area around the outlet of the reference (inner) Pt wire, but this seal is localized and does not encompass the circumference of the joining plane. Using this novel sealing method, a sensor package has been developed wherein a metal/metal oxide solid mixture provides a reference $pO_2$ for high temperature oxygen sensing applications. The solid mixture is not placed in contact with the internal electrode, preventing unfavorable reactions that could lead to signal anomalies [8]. The fabricated sensor, a pellet 10 mm in diameter and ∼5 mm thick, exhibits fast response and reproducible sensing characteristics. Seals created by directly fusing zirconia package components are inherently free of bonding agents and do not interfere with sensor operation. Leak faults induced by thermal expansion mismatch over temperature cycling and long periods of time are similarly eliminated. In the temperature window of operation, 600–700 °C, oxygen leak through electronic conduction is the sole detectable source of leak and can be eliminated through a brief electrochemical treatment.

## 2. Experimental

### 2.1. Sensor assembly

The package superstructure was constructed from the following materials and placed into the Instron Universal Testing Machine as demonstrated in Fig. 1. The electrolyte, ring and bottom wafer were cut from preformed and densified rods/tubes of 3 mol% yttria-stabilized tetragonal zirconia polycrystals (YTZP, average particle size ∼0.4 μm) that were purchased from Custom Technical Ceramics, Inc. (Arvada, CO). The 8 mol% cubic yttria-stabilized zirconia spacers (YSZ, average particle size ∼8 μm) were cut from a rod that was also purchased from Custom Technical Ceramics, Inc. The YTZP green tapes (Nextech, Columbus, OH) were laser cut from sheets into rings the area of which matched that of the YTZP ring. The Pt wire to the inner reference electrode was sandwiched between two pieces of YTZP green tape. The devices were constructed by sealing 100% metal oxide into the reference chamber (PdO, $RuO_2$, NiO, obtained from Alfa Aesar). A small amount of 8 mol% YSZ powder (TZ-8Y, Tosoh, Japan) was placed on top of the metal oxide to prevent alloying with the Pt wire of the reference electrode.

Each "sandwich" was compressed in an argon atmosphere at temperatures ranging from 1250 to 1290 °C in a universal testing machine (Instron, Model 1125) at crosshead speeds ranging from 0.01 to 0.02 mm/min. In order to avoid overstressing the sample and possibly damaging the Pt wire, the strain rate used for all experiments was $4 \times 10^{-5}\,s^{-1}$. In the >1250 °C temperature domain, this strain rate is expected to yield total stresses on a 1 $cm^2$ sample of less than 40 MPa [10]. During the heating cycle, the load on the sample was balanced as not to exceed 5 N. Upon reaching the target temperature, the system was left under a 5 N load for 30 min to attain thermal equilibrium.

Following joining, a glass plug was applied to the region of the sensor package where the Pt wire breached the inner-to-outer environment (C153M Glass, Asahi, Japan—softens at 800 °C, crystallizes at 910 °C). C153M is a frit sealing glass composed

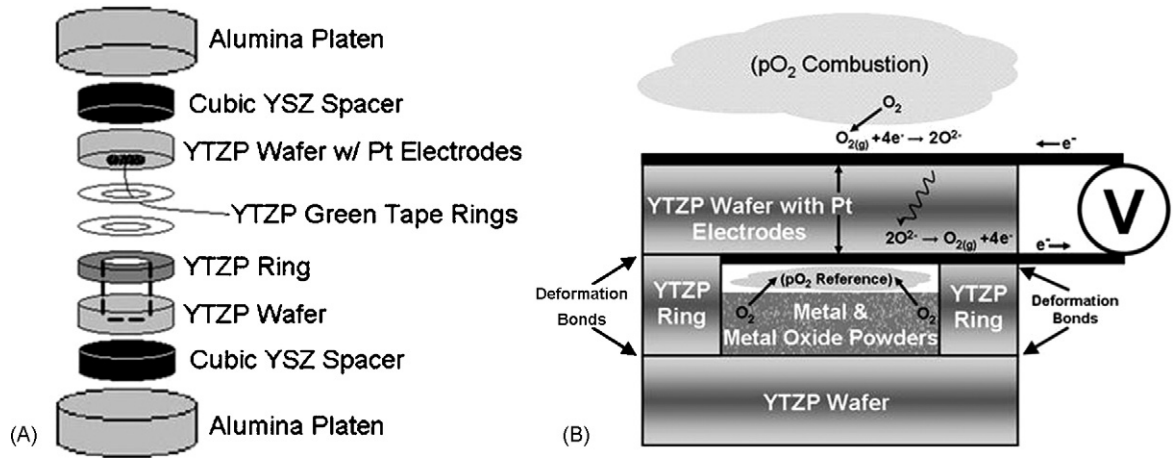


Fig. 1. (A) Components of the sensor package. The cup in which the metal/metal oxide powder was placed was formed by placing a YTZP ring on top of a YTZP wafer. The cubic YSZ spacers were necessary as bonding occurred between YTZP and alumina during initial joinings. Cubic YSZ spacers and alumina platens were removed following joining and not part of the $O_2$ sensor. (B) Sensor schematic.

of $SiO_2$, ZnO and organic compounds. The glass powder was mixed with α-terpineol to make a slurry and a small amount was applied to the base of the Pt wire. The sensor was heated to 1200 °C for 3 h to densify the glass plug.

### 2.2. Electrical measurements

In order to collect open circuit potentials, the devices were placed in a quartz cylinder housed at the center of a tube furnace and attached via platinum leads to a Hewlett-Packard HP34970A multiplexer. The multiplexer was operated in low internal impedance mode (∼10 MΩ). Sensor temperature was assumed as the set point of the furnace. Upon thermal stabilization, the open circuit potential was measured every 5 s. The sensor exhibits stability on the order of months. Equipment demand limitations prevented testing for greater periods of time, but the sensor demonstrated no sign of failure during the long-term tests. Sensitivity to changes in external $pO_2$ was tested at 600 and 700 °C at six different oxygen concentrations: 3%, 5%, 7%, 10%, 14%, 21% relative percent, balanced in $N_2$. The flow of gases used was determined with digital mass flow controllers manufactured by Sierra.

All sensitivity to external $pO_2$ concentration changes was collected in pump-out mode: the negative terminal attached to the inner electrode and the positive terminal attached to the external electrode.

Electrochemical pumping at 700 °C and 21% oxygen was enabled through Gamry Instruments Potentiostat with software control operating in galvanostatic mode at 100 μA. As the sensor is a two-electrode cell it is not possible to measure an accurate open circuit potential during or directly after electrochemical pumping due to the cathodic overpotential introduced during the pump [12]. Therefore, following the pumps, the system was relaxed for a minimum of 1 h to allow excess charge to dissipate.

### 2.3. Characterization techniques

SEM micrographs were obtained using a Philips XL-30 ESEM. In order to view the joints, sensors were cross-sectioned, polished, and thermally etched in air at 1200 °C for 3 h to reveal the grains. Following etching, the samples were mounted onto aluminum pegs with double-sided carbon tape and coated with evaporated gold.

X-ray photoelectron spectroscopy (XPS) studies were performed with a Kratos AXIS Ultra X-ray photoelectron spectrometer. An Al source was used for all measurements. Experiments were performed at a resolution of 0.1 eV with a pass energy of 20 eV. The Pd and PdO powders used to construct the sensors were used to get reference binding energy values. Charge balancing was used to eliminate charging of the sample during measurement.

The X-ray diffraction (XRD) patterns were determined with a Bruker D-8 X-ray diffractometer using nickel-filtered Cu Kα (λ = 1.5405 Å) radiation.

## 3. Results

### 3.1. Degree of compression and microstructure of fused package

The metal/metal oxide combinations used in construction of the sensor devices were placed into the "cup" created by the bottom wafer and ring as demonstrated in Fig. 1. Load and time were monitored during the heating cycle and the compression cycle. During compression, stresses ranged from 3.2 to 6.4 MPa. Each device package was compressed to a target of 90–93.5% of its initial height. During the compression, a steady-state stress indicated by a strain-independent stress was achieved [13]. The results of this compression are presented in Table 1.

SEM micrographs of the joints produced for the Ni/NiO-containing package at 1250 °C/5.7 MPa are presented in Fig. 2. Fig. 2A presents a cross-sectional view of a cut made approximately 1 mm from the edge of the sensor, while Fig. 2B presents a cross-sectional view of a cut made approximately 3 mm from the edge of the sensor. The joining planes are indistinguishable from the bulk ceramic and exhibit no poros-

Table 1
Temperature and compression parameters

| Sensor reference material | Temperature upon application of load (±3 °C) | Initial height (mm) | Final height (mm) | Percent longitudinal compression (%) | Stress (MPa) |
|---|---|---|---|---|---|
| Ni/NiO | 1245 | 7.6 | 6.9 | 9.0 | 5.7 |
| $Ru/RuO_2$ | 1275 | 5.0 | 4.7 | 6.1 | 6.4 |
| Pd/PdO | 1250 | 5.0 | 4.8 | 4.7 | 3.2 |

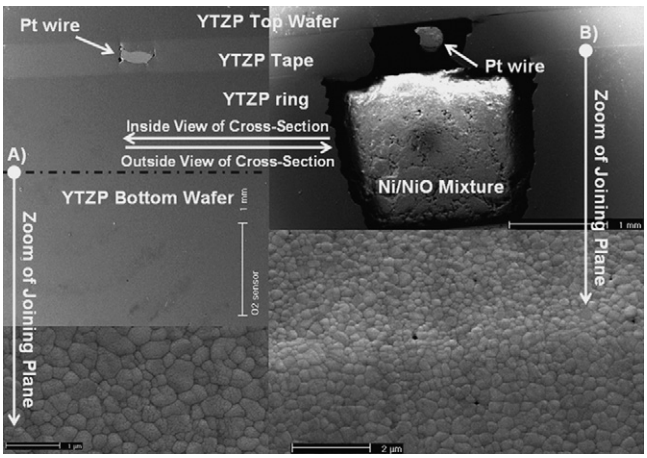


Fig. 2. Cross-sectional view of a Ni/NiO sensor assembly. In (A) the piece that was liberated exhibits poor sealing around the Pt-wire, but good sealing in all other areas. The zoom highlights the efficacy of the bottom ring-to-wafer joint. In (B) the bulk of the remaining sensor shows the state of the Ni/NiO solid reference and the non-contact between the reference material and the Pt-wire. The zoom highlights the efficacy of the YTZP tape to YTZP ring joint.

ity. Packages pressed at 1250 °C/3.2 MPa exhibit similarly pore-free YTZP/YTZP joining planes. The YTZP/Pt joining regime, where the Pt reference electrode lead breaches the inner-to-outer environment, is marked by micrometer-scale imperfections. These imperfections are presented in a view of the wire amidst densified green tape in Fig. 3. A plug of C153M glass was applied to this imperfect region around the Pt wire.

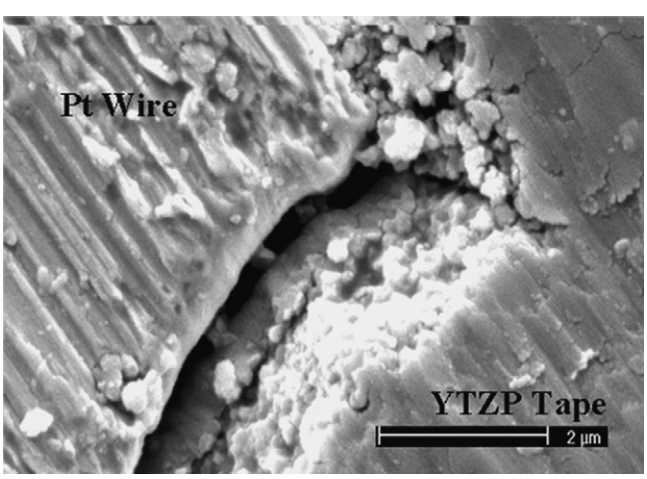


Fig. 3. Cross-sectional view of a Pd/PdO-based sensor, 1 mm from the edge where the Pt-wire breached the inner-to-outer environment. The 1 μm fissure is the localized area where the glass plug was applied.

### 3.2. Efficacy of joint at various temperatures and thermal cycling

In an attempt to test the durability of the fused package, the Pd/PdO containing device was thermally cycled over the course of 8 days. The temperature was changed every 5 h to 700, 600, 500, 400, 300, 200, 100, 25, and then back to 700 °C. The voltages recorded during thermal cycling are presented in Fig. 4 and demonstrate that sensor responses from all cycles overlap. These thermal cycling tests indicate no $O_2$ leak during the 8 days of constant monitoring. The thermal cycling test was repeated four times and the voltage measured at 21% $O_2$ was within 1% of the value from the previous test periods.

The Pd/PdO-containing device was subjected to an 80 h, 800 °C temperature treatment. Fig. 5 contains sensor traces for the first 48 h at 800 °C as well as the first 48 h after the temperature was lowered to 700 °C. Failure of the device occurs at approximately 40 h at 800 °C. Beyond this time, the open circuit potential drifted to 0 V. Upon cooling to 700 °C, sensitivity was completely restored.

### 3.3. Sensor characteristics

#### 3.3.1. Studies with different metals/metal oxides

Table 2 compares the air background open circuit potentials measured with the Ni/NiO, Pd/PdO and $Ru/RuO_2$ at various temperatures. The theoretical pressures and sensor responses

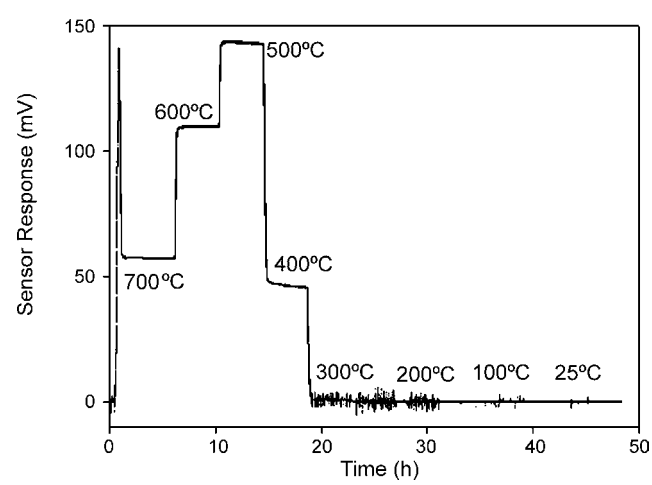


Fig. 4. Thermal cycling of the Pd/PdO-based oxygen sensor. The sensor was subjected to a new temperature every 5 h for a 40 h period. This was repeated four times. The sensor responses over these four test periods overlapped. The initial voltage spike is the sensor response as the tube furnace heats the sensor from room temperature to 700 °C.

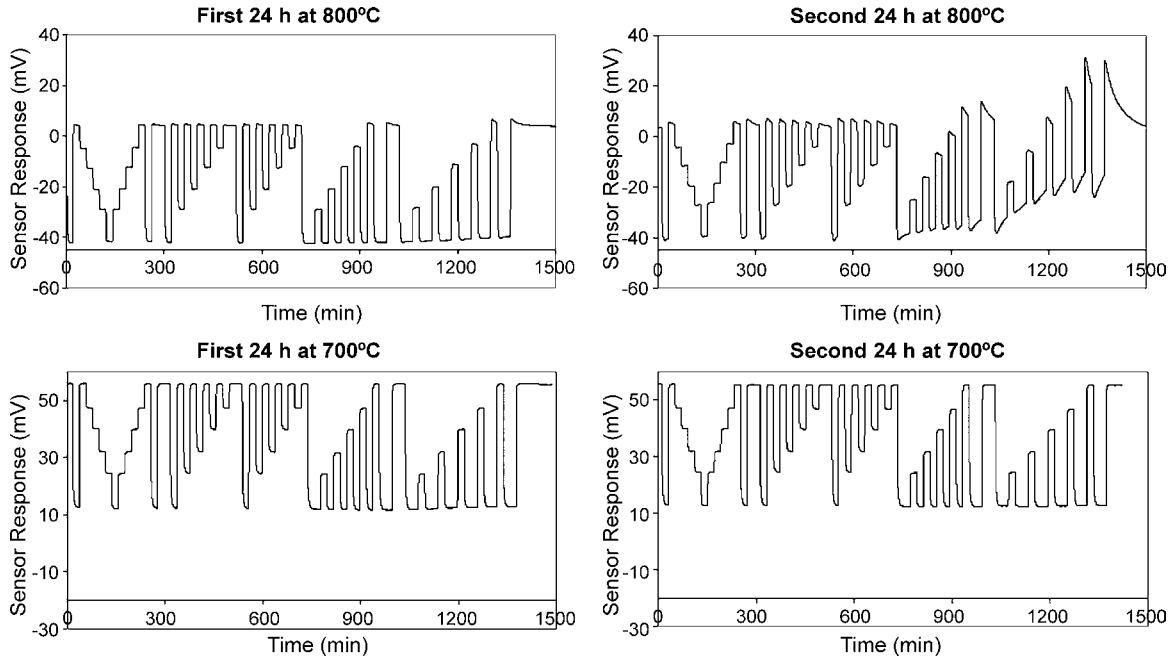


Fig. 5. Thermal studies of Pd/PdO-based sensor at 800 °C. Frames (A) and (B) are the first 48 h of an 80 h test. Frames (C) and (D) are the 48 h following the 80 h test wherein the temperature was dropped to 700 °C. Sensitivity was degraded after approximately 24 h at 800 °C and lost after approximately 48 h at 800 °C. Sensitivity was restored and maintained when the temperature was lowered to 700 °C.

Table 2
Experimental and theoretical sensor responses

| Oxide reference | Temperature (°C) | $\Delta G^\circ$ (kJ) | Theoretical pressure (atm) | Theoretical 21% $O_2$ sensor response (mV) | Observed pressure (atm) | Observed 21% $O_2$ sensor response (mV) |
|---|---|---|---|---|---|---|
| NiO | 600 | −317.04 [14] | $1.1 \times 10^{-19}$ | 792.1 | $1.3 \times 10^{-19}$ | 788.0 |
| NiO | 700 | −297.33 [14] | $1.1 \times 10^{-16}$ | 737.6 | $2.6 \times 10^{-18}$ | 732.0 |
| $RuO_2$ | 600 | −154.84 [15] | $5.5 \times 10^{-10}$ | 371.8 | $1.3 \times 10^{-8}$ | 311.9[a] |
| $RuO_2$ | 700 | −137.73 [16] | $4.0 \times 10^{-8}$ | 324.1 | $6.1 \times 10^{-8}$ | 315.7 |
| PdO | 600 | −52.65 [16] | $7.1 \times 10^{-4}$ | 107.0 | $6.2 \times 10^{-4}$ | 109.6 |
| PdO | 700 | −32.92 [16] | $1.7 \times 10^{-2}$ | 52.5 | $1.4 \times 10^{-2}$ | 56.5 |

[a] Seal on this sensor was not optimal.

in Table 2 were calculated using the most recently published [14–16] $\Delta G$ values and the Nernst equation. The inner volume was approximated to be 28 $mm^3$. Fig. 6 shows the open circuit potential measurements of all fused packages as the external $O_2$ concentration is changed. The current flow through the electrolyte induced by measurement of the voltage pumps oxygen into or out of the reference chamber, resulting in an electrochemical leak. In low internal impedance mode, this electrochemical leak is manifested as an $O_2$ pump rate of $\sim 10^{-4}$ atm/h. The background signal drifts due to the electrochemical leak in a 12 h time period for the devices with Ni/NiO, Ru/$RuO_2$ and Pd/PdO in Fig. 6 were 0.0013%, 0.0075% and 0.0009%, respectively. As seen in Table 2, the Pd/PdO-containing device exhibits the highest internal oxygen pressure and therefore is expected to be maximally resistant to the electrochemical leak induced by measurement.

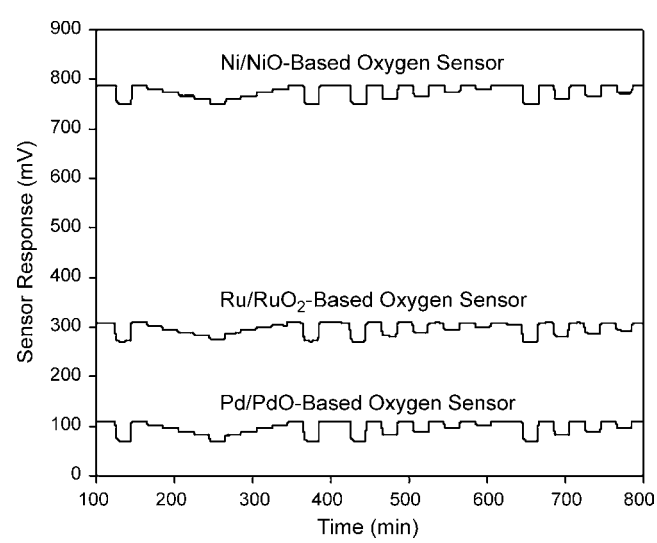


Fig. 6. Sensor traces of Pd/PdO, Ru/$RuO_2$, and Ni/NiO containing oxygen sensors at 600 °C.

### 3.3.2. Drift

The Pd/PdO-containing sensor was subjected to a drift test at 700 °C in 21% oxygen with data collection every 5 s for

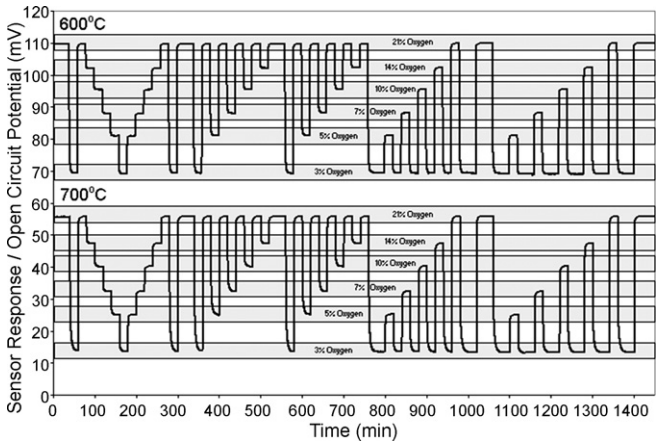


Fig. 7. Performance of the Pd/PdO-based sensor at 600 and 700 °C to changing external oxygen concentrations.

214 consecutive hours. Over this test period the sensor exhibited a maximum signal deviance of 0.93 mV, corresponding to a pressure deviation of $6.5 \times 10^{-4}$ atm—or 0.3% of the baseline pressure. The minimum-recorded sensor response was 55.23 mV and the maximum response was 56.16 mV. The average response was 55.66 mV.

### 3.3.3. Sensitivity

Fig. 7 highlights the sensitivity of the Pd/PdO-containing sensor to changes in external oxygen concentration over 24 h at 600 and 700 °C. In a 192 h period there is no baseline drift at 700 °C and a 1.5% baseline drift at 600 °C. While the background signals changed at 600 °C, there was no loss of sensitivity at any point during the experiment. Over the 8-day test cycle the sensor exhibited near-Nernstian sensitivity at 600 and 700 °C. Table 3 lists the slopes of the Nernstian sensitivity plots (sensor response versus $\log pO_2$) of two Pd/PdO-containing sensors. One of the possible reasons for deviation from Nernstian sensitivity is that the temperature experienced by the sensor is slightly different from the furnace setting.

### 3.3.4. Cross-sensitivity

The Pd/PdO-containing sensor was subjected to a cross-sensitivity test to 250–900 ppm of CO and 2–10% of $CO_2$. The cross-sensitivity to these gases is presented in Fig. 8. $E/E_0$ is defined as the response to a given concentration ($E$) divided by the baseline response ($E_0$). In frame (A), the baseline is defined as the sensor response to 21% $O_2$. In frames (B) and (C) the baseline is defined as the sensor response to 10% $O_2$ in the absence of the interferent gas. At 600 °C, the CO interference would lead to a false negative for oxygen of 1.1% and 3.2% at 250 and 900 ppm CO, respectively. There is no measurable sensor response to 2–10% $CO_2$ at 600 °C.

Table 3
Nernst slopes of Pd/PdO-based sensor at 600 and 700 °C

| | Pd/PdO sensor I (600 °C) | Pd/PdO sensor I (700 °C) | Pd/PdO sensor II (700 °C) |
|---|---|---|---|
| Day 1 | 46.96 | 52.02 | 49.93 |
| Day 2 | 47.08 | 51.07 | 50.48 |
| Day 3 | 46.43 | 52.01 | 49.55 |
| Day 4 | 47.04 | 51.17 | 49.93 |
| Day 5 | 47.55 | 50.84 | 49.99 |
| Day 6 | 47.69 | 50.38 | 49.84 |
| Day 7 | 48.28 | 50.46 | 50.14 |
| Day 8 | 45.95 | 49.98 | 50.2 |
| Theoretical Nernst slope | 43.32 | 48.27 | 48.27 |

### 3.4. Buffering action

In the long-term, all sensors operated in a single direction pump mode will enter a state where either the metal or metal oxide is completely depleted, inhibiting sensor performance. Long-term operation was simulated by electrochemical pumping at currents five orders of magnitude greater than the input bias current in a typical sensor experiment. In this manner the sensing electrodes were briefly used as pumping electrodes as in an oxygen pump-gauge [4,7]. In short times it is possible to move large quantities of oxygen through the electrolyte—simulating the oxygen concentration changes that arise as a consequence of normal long-term operation.

Prior to electrochemical pumping, the baseline voltage was 56.5 mV at 700 °C, corresponding to an internal oxygen pressure of $1.4 \times 10^{-2}$ atm. After 48 h of electrochemical out-pumping at 0.1 mA, the sensor exhibited a baseline voltage of 1.75 V at 700 °C, corresponding to an internal oxygen pressure of $1.2 \times 10^{-37}$ atm. Oxygen was electrochemically pumped into the sensor for 1 h to determine if the equilibrium $O_2$ pressure could be restored. Following the 1 h pump-in at 0.1 mA, the baseline was re-established at 56.5 mV.

After 7 days of 24 h pump-ins at 0.1 mA, the background voltage rose to −80.7 mV, corresponding to an internal oxygen pressure of 9.9 atm. At this time the sensor was destroyed for X-ray analyses. In the Pd $3p_{3/2}$ and Pd $3p_{1/2}$ regions of the pumped-in sample the X-ray photoelectron spectroscopy (XPS) peak positions in Fig. 9 are at 561.5 and 533.7 eV, respectively. There is also an observable shoulder in the 533.7 eV peak. There is a well-defined O 1s peak at 530.2 eV. Literature indicates that for Pd metal, the Pd $3p_{1/2}$ peak is found at 560.2 eV and the Pd $3p_{3/2}$ peak is found at 532.4 eV [17]. The Pd metal powder used in this study exhibited Pd $3p_{3/2}$ and Pd $3p_{1/2}$ peaks at 560.3 and 532.5 eV, respectively. Literature also indicates that in PdO, the Pd $3p_{1/2}$ peak can be found at 562.1 eV and the Pd $3p_{3/2}$ peak at 534.2 eV [18]. The PdO powder used in the construction of the Pd/PdO-containing sensor exhibits Pd $3p_{3/2}$ and Pd $3p_{1/2}$ peaks at 561.9 and 534.1 eV, respectively. In the X-ray powder diffraction (XRD) of the pumped-in sample presented in Fig. 10, the five major peaks at 33.6°, 41.7°, 54.5°, 59.9° and 71.1° indicate a majority of PdO [19]. There is a minor peak at 40.0°, the most intense line of Pd metal. Thus, both XRD and XPS indicate a minority of metallic palladium in the sample.

Pd/PdO recovered from a sensor that was operated for >1000 h was also analyzed by XPS and XRD. The XPS peak positions for the Pd $3p_{3/2}$ and Pd $3p_{1/2}$ orbitals from the long-

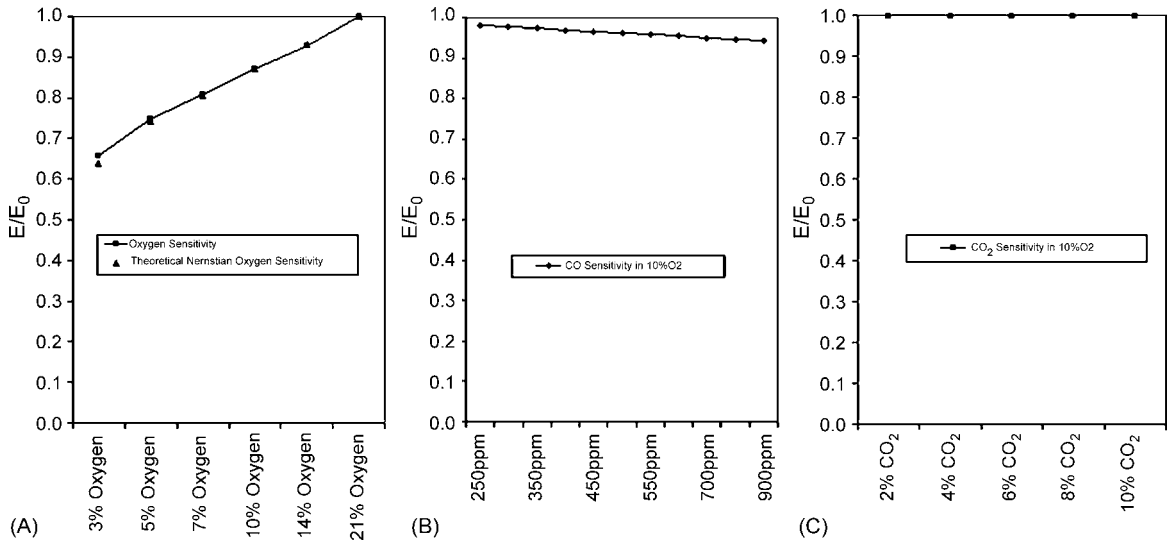


Fig. 8. Cross-sensitivity of Pd/PdO-based sensors at 600 °C. Oxygen sensor sensitivity to changing (A) oxygen concentration, (B) CO concentration in a background of 10% $O_2$, and (C) $CO_2$ concentration in a background of 10% $O_2$.

term pumped-out operation sensor presented in Fig. 11 are 560.0 and 532.2 eV, respectively. In the characteristic XRD $2\theta$ region of 20°–80° of the pumped out sample presented in Fig. 12, the three intense peaks at 39.75°, 46.30°, and 67.75° indicate a majority of Pd metal [20]. The minor peak at 34.5° is attributed to PdO. A minor shoulder at ∼530 eV in the XPS, typical of O 1s, indicates a small amount of PdO. This is consistent with the XRD data. The three peaks at 29.70°, 49.9°, and 59.3° are due to the presence of the 8 mol% YSZ that was added on top of the reference metal/metal oxide to prevent alloying with the internal electrode. These YSZ peaks are not observed in Fig. 10 because a different portion of the reference material was analyzed.

## 4. Discussion

### 4.1. Moving from YSZ to YTZP

Cubic YSZ is used for most oxygen sensors as its high ionic conductivity above 400 °C allows for efficient use as an electrolyte [5]. However, first attempts to join two discrete pieces of cubic YSZ failed as its crystal structure precludes it from achieving plasticity at temperatures and loads within the capability of the Instron. Plastic deformation resulting from grain boundary sliding is strongly dependent on the grain size and the forces necessary to induce creep would destroy the sample before plastic deformation could occur [21,22]. YTZP is not

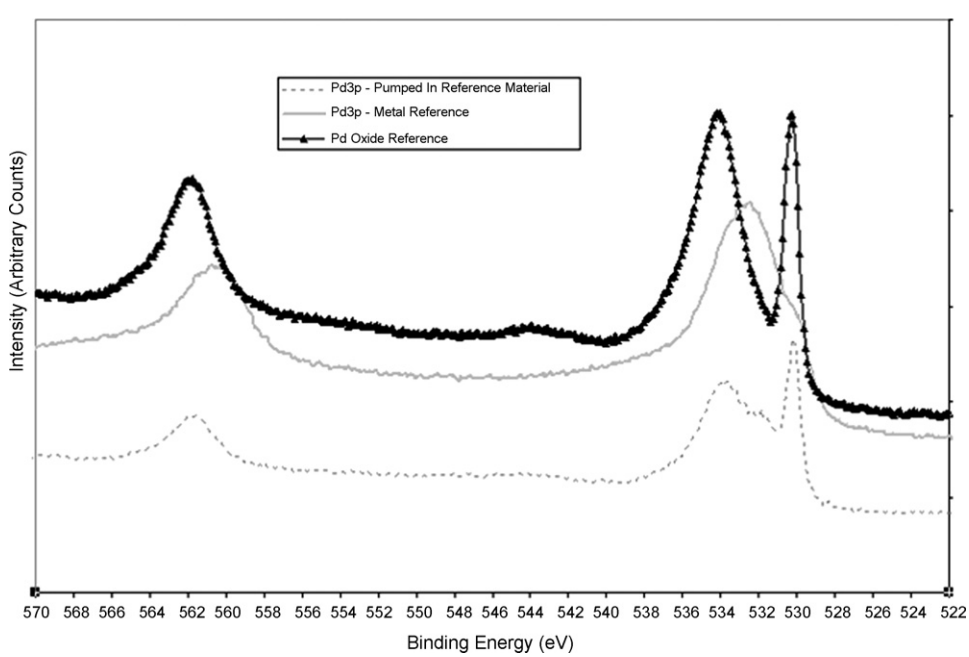


Fig. 9. XPS of metal/metal oxide recovered from the electrochemically pumped-in Pd/PdO-containing oxygen sensor, Pd-metal reference, and PdO reference. The spectra indicate that the majority of the Pd has been oxidized during the electrochemical pumping-in.

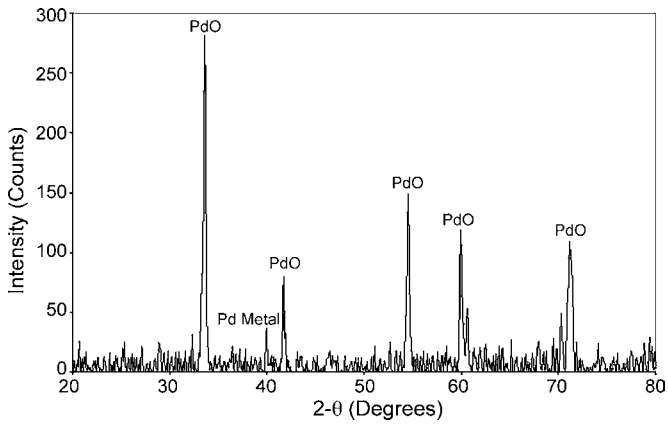


Fig. 10. XRD of metal/metal oxide recovered from Pd/PdO-containing oxygen sensor that was electrochemically pumped-in. The majority PdO peaks and small Pd-metal peak indicate a majority of oxidized Pd after subjection to electrochemical pumping-in.

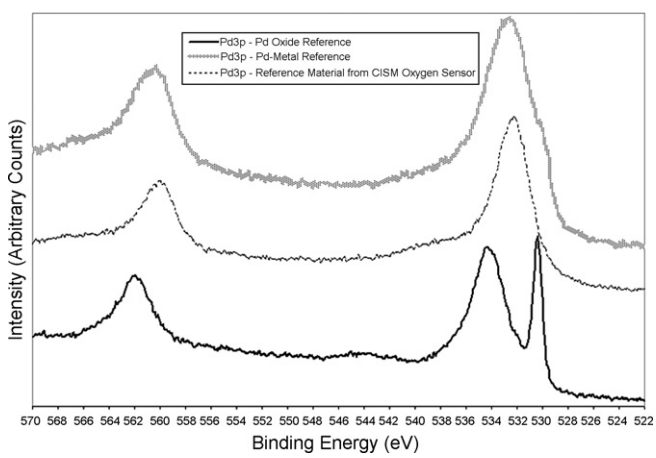


Fig. 11. XPS of metal/metal oxide from the 1000+ h of pump-out operation Pd/PdO-containing oxygen sensor, Pd-metal reference, and PdO reference. The spectra indicate that there is very little oxidized Pd remaining after long-term pumping-out mode operation.

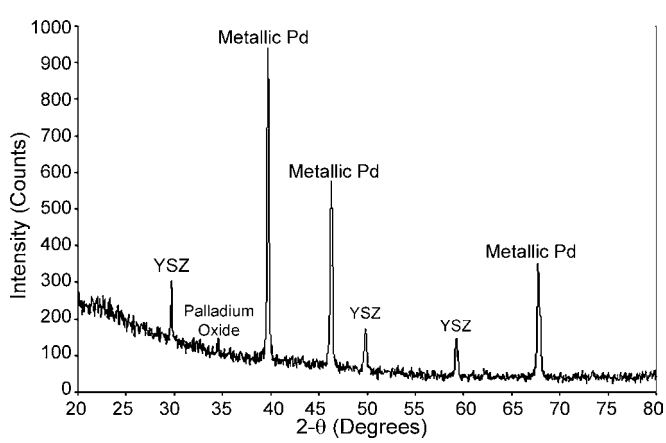


Fig. 12. XRD of metal/metal oxide recovered from Pd/PdO-containing oxygen sensor operated for 1000+ h in pumping-out mode. The majority Pd-metal peaks and small peak where the major PdO peak is found indicate a majority of Pd-metal after long-term pumping-out mode operation. The YSZ present in this diffraction pattern was added to prevent alloying between the inner Pt-electrode and the reference Pd/PdO.

commonly used as an electrolyte for solid-state oxygen sensors as its ionic conductivity is below that of its cubic counterpart. Badwal and Swain [23] highlight the low grain boundary conductivity of YTZP—noting that it is generally considered an unsuitable electrolyte. Results by Ramasamy and colleagues [24] contradict this conclusion and indicate that for fine grained YTZP the grain boundary conductivity may be higher in YTZP than coarser grained YSZ. However, Ramasamy and colleagues [24] also notes that overall dc-conductivity remains an order of magnitude lower, even in fine-grained samples. Regardless of the overall conductivity, the performance of the sensor above 600 °C, as shown in Fig. 6, indicates the sub-micron grained YTZP is a suitable electrolyte for Nernst-type oxygen sensors.

### 4.2. Seal efficacy—role of glass

The durability of the seal was probed by monitoring the open circuit potential as a function of time during thermal cycling. The thermal cycling tests indicate that there is no evidence of leak during the 8 days of constant monitoring. The 48 h thermal cycling was repeated four times and the background air voltage was within 1% of the value from the previous test period.

When the temperature is raised to 800 °C, the softening point of the glass, the seal around the inner electrode lead wire is strained. As evidenced in Fig. 5, the seal serves as an effective gas barrier for approximately 40 h. Eventually, the glass softens sufficiently to act as a semipermeable membrane. The gas flow through the softened seal is not so rapid as to cause instantaneous equilibrium, but rather serves as an imperfect barrier that prevents equilibration of the internal/external environments for tens of hours. Upon cooling to 700 °C, the voltage measured, 55.5 mV indicates the pressure inside the device was restored to equilibrium levels within 40 min. The implication of the restoration of sensitivity is that while the seal is compromised at temperatures >800 °C, this sealing effect is rectified by lowering the temperature and allowing time for the metal/metal oxide reference material to re-establish equilibrium with the oxygen that flowed in during exposure.

### 4.3. Role of internal oxygen pressure

As demonstrated in Fig. 6, different metal/metal oxide combinations will generate different $O_2$ pressures within the reference chamber. Ni/NiO, Pd/PdO, and Ru/$RuO_2$ were selected for study as they did not melt at the joining temperatures and represented relatively low, medium and high pressures of oxygen when heated to the temperature regime of interest, between 600 and 800 °C. The magnitude of the internal pressure is a consideration for selecting an appropriate measuring device and the long-term operation of the sensor.

The importance of selecting an appropriate measuring device was apparent when a noticeable drift was observed in the air background signals of both the Ni/NiO and Ru/$RuO_2$ sensors. As calculated from Fig. 6, this drift is attributed to $O_2$ being pumped into or out of the sensor when operating the HP34970A in low internal impedance mode (10 MΩ). In low internal impedance mode, the HP34970A was subjected to an

Table 4
Observed pressure rises during operation of the Pd/PdO-based sensor

| Temperature (°C) | Time of test (h) | Initial pressure (atm) | Final pressure (atm) | Increase factor (%) | Pressure rise (atm) | Expected rise (atm)[a] |
|---|---|---|---|---|---|---|
| 600 | 232.9 | $6.1 \times 10^{-4}$ | $6.2 \times 10^{-4}$ | 1.5 | $9.4 \times 10^{-6}$ | $7.9 \times 10^{-3}$ |
| 700 | 329.0 | $1.4 \times 10^{-2}$ | $1.4 \times 10^{-2}$ | 0 | 0 | $1.3 \times 10^{-2}$ |

[a] Calculated from values presented in Table 2.

input bias current in the range of tens of nanoamperes. At 600 °C this amounts to $\sim 10^{-12}$ mol oxygen per hour of operation (assuming a measurement is taken every 5 s). Using the approximate inner volume of 28 $mm^3$, the pressure rise during low impedance operation is calculated to be $\sim 10^{-4}$ atm/h. Even though the metal/metal oxide will buffer the oxygen concentration changes, the Ni/NiO sensor exhibits an initial pressure of $10^{-19}$ atm at 600 °C (Table 2). Such an electrochemical leak will lead to drifts in either pump-in or pump-out mode. This phenomenon is also present in the $Ru/RuO_2$ oxygen sensor. At 600 °C $Ru/RuO_2$ exhibits an internal pressure of $\sim 10^{-8}$ atm (Table 2). Using the same approximated internal volume, pumping at $\sim 10^{-4}$ atm/h will rapidly perturb the equilibrium such that a steady baseline cannot be obtained. Operating the HP34970A in high internal impedance mode (>10 GΩ) vastly reduced this effect. This was confirmed by testing the Ni/NiO sensor at 600 °C in high internal impedance mode. In a 24 h period, there was no noticeable drift in the sensor signal in the presence of air.

The second issue when considering the magnitude of the internal pressure is the reliable long-term operation of the sensor. In either high or low internal impedance mode, a sensor is stable when the equilibrium $O_2$ pressure generated by the metal/metal oxide is large relative to the electrochemical leak. In this manner, any oxygen that enters or leaves the package within a measurement timeframe is insignificant relative to the internal pressure and will not affect the sensitivity of the measurement. Therefore, the optimum metal/metal oxide for use within a sensor is determined by the target temperature of the application. For example, at 600 °C, Pd/PdO is a suitable reference as its equilibrium $O_2$ pressure is higher than the electrochemical leak rate in low internal impedance mode. At 700 °C or in high internal impedance mode, the electrochemical leak rate is significantly below the equilibrium pressure. Were the temperature to be raised as high as 1200 °C, Pd/PdO would no longer be a suitable reference, since the sensor would not be able to buffer incoming oxygen by oxidizing Pd metal. On the other hand, at 1200 °C Ni/NiO would be a more suitable reference material since it can buffer changes in $O_2$ concentration incurred by measurement.

### 4.4. Exploiting the joint quality to make a stable sensor

The efficacy of the seal in resisting the strain of thermal cycling and high temperature operation makes it possible to hold extremely small concentrations of $O_2$ inside the sensor package. For this reason, the electrochemical leak is a concern when using a simple measuring system. Of the three combinations screened in low internal impedance mode, Pd/PdO was the best for use in the 600–800 °C temperature regime. Pd/PdO exhibits negligible drift in the 600–700 °C temperature regime because its equilibrium oxygen pressure is above the magnitude of electrochemical leak in both high and low internal impedance modes.

Table 4 presents the observed background pressures, pressure rises and expected pressure rises for the Pd/PdO-containing sensor. In the 600 °C Pd/PdO-based sensor trace presented in Fig. 6, drift is barely perceptible and over the course of 233 h the internal pressure rises by just 1.5%. In the 700 °C sensor traces the internal pressure is three orders of magnitude greater than the expected pressure rise, and therefore has little effect on the sensor drift. This effect is noted in the stability of the sensor background response to 21% oxygen over 329 h at 700 °C.

As the physical leakage has been eliminated, long-term operation in the Pd/PdO-based device is controlled by the reaction $Pd + 1/2O_2 \Leftrightarrow PdO$. As demonstrated by the phase/oxidation state changes presented in Figs. 9–12, the sensor will continue to operate as long as it is possible for the system to reach equilibrium. Once Pd metal is exhausted in pump-in mode, or PdO exhausted in pump-out mode, the sensor will fail to operate properly as attaining equilibrium is no longer possible. However, the facility of electrochemically moving oxygen into/out-of the package indicates that even in long-term single mode operation, sensitivity can be readily restored.

## 5. Conclusion

A deformation-induced grain boundary sliding mechanism enabled a method for sealing an oxygen sensor with an internal metal/metal oxide reference. The sensor exhibits long-term stability. A variety of metal/metal oxide references can be used to construct oxygen sensors employing this seal. The reference metal/metal oxide serves as an effective source/sink for invading/escaping oxygen over the course of long-term operation. Operation under low-impedance, single-mode conditions will inhibit sensor performance in the very-long term. However, it has been demonstrated that the reference pressure can be restored and maintained with a brief electrochemical treatment. Selecting an appropriate metal/metal oxide reference material to embed in the sensor marginalizes the electrochemical leakage so that simple measuring electronics can be employed, as demonstrated with Pd/PdO at temperatures up to 700 °C. The prime hurdle to internal-reference sensors has been overcome—creating an effective physical seal.

Once good sealing against physical leakage is established, it is possible to use the deformation joining mechanism to create sensors that are tunable for a particular temperature window

of operation. Work continues to adapt the deformation joining technique so that glass sealing around the internal Pt electrode wire is no longer necessary and operation temperatures can be raised past 800 °C. In this manner, the temperature-tunable oxide operation paradigm can be further investigated.

As the sensor does not require reference gas plumbing, there is more flexibility in placement of sensors in a combustion stream. Furthermore, the sensor assembly process readily lends itself to miniaturization.

## Acknowledgements

The work at Argonne National Laboratory was supported by the Office of FreedomCAR and Vehicle Technologies of the U.S. Department of Energy, under Contract No. W-31-109-Eng. The work at The Ohio State University was supported by the Department of Energy (DE-FC26-03NT41615). We acknowledge the help of Dr. Chonghoon Lee and Pengbei Zhang of The Ohio State University for their assistance in generating cross-sensitivity data.

## References

[1] D. Linkins, D. Lewis, R. Frank, J. Weiss, TVA's Kingston Unit 9 Distributed Control System (DCS) retrofit benefit documentation, TVA Tech. Adv. 1 (1997) 69–75.
[2] R. Ramamoorthy, P.K. Dutta, S.A. Akbar, Oxygen sensors: materials, methods, designs and applications, J. Mater. Sci. 38 (2003) 4271–4282.
[3] W.C. Maskell, B.C.H. Steele, Solid state potentiometric oxygen gas sensors, J. Appl. Electrochem. 16 (1986) 475–489.
[4] J. Fouletier, G. Vitter, M. Kleitz, Measurement and regulation of oxygen content in gases using solid electrolyte cells. III. Oxygen pump-gauge, J. Appl. Electrochem. 5 (1975) 111–120.
[5] D.M. Haaland, Internal-reference solid-electrolyte oxygen sensor, Anal. Chem. 49 (1977), 1813-11.
[6] W.C. Maskell, Progress in the development of zironica gas sensors, Solid State Ionics 134 (2000) 43–50.
[7] H. Kaneko, T. Okamura, H. Taimatsu, Y. Matsuki, H. Nishida, Performance of a miniature zirconia oxygen sensor with a Pd–PdO internal reference, Sens. Actuators B 108 (2005) 331–334.
[8] S. Zhuiykov, '*In Situ*' diagnostics of solid electrolyte sensors measuring oxygen activity in melts by a developed impedance method, Meas. Sci. Tech. 17 (2006) 1570–1578.
[9] E. van Setten, T.M. Gur, D.H.A. Blank, J.C. Bravman, M.R. Beasley, Miniature Nernstian oxygen sensor for deposition and growth environments, Rev. Sci. Instrum. 73 (2002) 156–161.
[10] F. Gutierrez-Mora, K.C. Goretta, S. Majumdar, J.L. Routbort, M. Grimdisch, A. Dominguez-Rodriguez, Influence of internal stresses on superplastic joining of zirconia-toughened alumina, Acta Mater. 50 (2002) 3475–3486.
[11] F.A. Mohamed, Y. Li, Creep and superplasticity in nanocrystalline materials: current understanding and future prospects, Mater. Sci. Eng. A 298 (2001) 1–15.
[12] A.Q. Pham, R.S. Glass, Oxygen pumping characteristics of yttria-stabilized-zirconia, Electrochem. Acta 43 (1998) 2699–2708.
[13] F. Gutierrez-Mora, A. Dominguez-Rodriguez, J.L. Routbort, R. Chaim, F. Guiberteau, Joining of yttria-tetragonal stabilized zirconia polycrystals using nanocrystals, Scripta Mater. 41 (1999) 455–460.
[14] H.St.C. O'Neill, Free energies of formation of NiO, CoO, $Ni_2SiO_4$, and $Co_2SiO_4$, Am. Mineral. 72 (1987) 280–291.
[15] H.St.C. O'Neill, J. Nell, Gibbs free energies of formation of $RuO_2$, $IrO_2$, and $OsO_2$: a high temperature electrochemical and calorimetric study, Geochim. Cosmochim. Acta 61 (1997) 5279–5293.
[16] J. Nell, H.St.C. O'Neill, Gibbs free energy of formation and heat capacity of PdO: a new calibration of the Pd–PdO buffer to high temperatures and pressures, Geochim. Cosmochim. Acta 60 (1996) 2487–2493.
[17] M.C. Militello, S.J. Simko, Elemental palladium by XPS, Surf. Sci. Spec. 3 (1997) 387–394.
[18] M.C. Militello, S.J. Simko, Palladium oxide (PdO) by XPS, Surf. Sci. Spec. 3 (1997) 395–401.
[19] JCPDS Powder Diffraction Database, PDF-number: 41-1107.
[20] JCPDS Powder Diffraction Database, PDF-number: 65-2867.
[21] A. Dominguez-Rodriguez, F. Gutierrez-Mora, M. Jimenez-Melendo, J.L. Routbort, R. Chaim, Current understanding of superplastic deformation of Y-TZP and its application to joining, Mater. Sci. Eng. A 302 (2001) 154–161.
[22] D. Singh, M. Lorenzo-Martin, G. Chen, F. Gutiérrez-Mora, J.L. Routbort, High-temperature deformation behavior in $SrTiO_3$ ceramics, J. Eur. Ceram. Soc., in press.
[23] S.P.S. Badwal, M.V. Swain, $ZrO_2$-$Y_2O_3$ electrical conductivity of some fully and partially stabilized single grains, J. Mater. Sci. Lett. 4 (1985) 487–489.
[24] R. Ramamoorthy, D. Sundararaman, S. Ramasamy, Ionic conductivity studies of ultrafine-grained yttria stabilized zirconia polymorphs, Solid State Ionics 123 (1999) 271–278.

## Biographies

**John V. Spirig** received his BS degree in Chemistry at the College of the Holy Cross in 1999. Before returning to graduate school he worked for 2 years at Wyeth Pharmaceuticals. He is currently a graduate student at The Ohio State University researching high temperature combustion sensors.

**Ramamoorthy Ramasamy** received his PhD degree in physics from University of Madras, India in 1999. He spent a year at the Technion-Israel Institute of Technology and 2 years at the University of Duisburg in Germany as an Alexander-von Humboldt postdoctoral fellow. From 2002 to 2005 he worked as a postdoctoral researcher at The Ohio State University. Currently, he is working at GE Advanced Materials as a Materials Scientist. His research interests are structural and electroceramics, glass-ceramic composites, high temperature non-oxide ceramics and gas sensors.

**Sheikh A. Akbar** is a Professor of Materials Science & Engineering and Founder of the NSF Center for Industrial Sensors and Measurements (CISM) at Ohio State University. He obtained his PhD degree from Purdue University in 1985. His current research focuses on microstructure-property relations of electroceramics (chemical sensors and fuel cell electrodes) both in bulk and thin-film forms.

**Jules Routbort** received his PhD in Engineering Physics from Cornell University in 1964. He was a postdoctoral fellow at the Cavendish Laboratory, Cambridge and at the Physics Department of Rensselaer Polytechnic Institute. He has been at Argonne National Laboratory since 1968 where his expertise is in the mechanical, diffusional, and fracture properties of materials. He is a Fellow of the American Ceramic Society, Iberdola Visiting Professor in the Condensed Matter Department of the University of Seville, adjunct Professor at Illinois Institute of Technology and North Carolina State University.

**Dileep Singh** is a Materials Scientist in the Nuclear Engineering division at Argonne National Laboratory. He joined Argonne as a postdoctoral fellow after receiving his PhD from University of Utah in 1991. His research interests include joining of materials, processing and mechanical characterization of ceramic materials and composites, and developing materials for nuclear waste containment.

**Prabir K. Dutta** received his PhD degree in Chemistry in 1978 from Princeton University. After 4 years of industrial research at Exxon Research and Engineering Company, he joined The Ohio State University, where currently he is the Robert K. Fox Professor and Chairman of the Department of Chemistry. His research interests are in the area of microporous materials, including their synthesis, structural analysis and as hosts for chemical and photochemical reactions.